Optical Flow for Flight and Wind Tunnel Background Oriented Schlieren Imaging

Nathanial T. Smith*
ACI/NASA Ames Research Center, Moffett Field, CA 94035, USA

James T. Heineck†, Edward T. Schairer‡
NASA Ames Research Center, Moffett Field, CA 94035, USA

Background oriented schlieren images have historically been generated by calculating the observed pixel displacement between a wind-on and wind-off image pair using normalized cross-correlation. This work uses optical flow to solve the displacement fields which generate the schlieren images. A well established method used in the computer vision community, optical flow is the apparent motion in an image sequence due to brightness changes. The regularization method of Horn and Schunck is used to create schlieren images using two data sets: a supersonic jet plume/shock interaction from the NASA Ames Unitary Plan Wind Tunnel, and a transonic flight test of a T-38 aircraft using a naturally occurring background, performed in conjunction with NASA Ames and Armstrong Research Centers. Results are presented and contrasted with those using normalized cross-correlation. The optical flow schlieren images are found to provided significantly more detail. We apply the method to an historical data set to demonstrate both the broad applicability and limitations of the technique.

I. Introduction

THIS work compares background oriented schlieren (BOS) images calculated from both normalized cross-correlation and a classical regularization-based optical flow method. Two data sets are used: supersonic wind tunnel data, and data from a transonic full scale flight test. The wind tunnel data is from the recent NASA plume/shock interactions study[1] conducted at the NASA Ames 9-by-7-ft. supersonic test section of the Unitary Plan Wind Tunnel (UPWT), and uses a Retroreflective BOS (RBOS) imaging technique. The flight test data is from a flight campaign conducted jointly by NASA Ames and NASA Armstrong research centers, and uses a natural background BOS technique to image a full-scale aircraft in flight.[2]

Whereas BOS images are generally computed using normalized cross correlation, this work uses optical flow, a computer vision technique, to generate the images. While this is not the first use of optical flow to generate background oriented schlieren images; to the authors' knowledge this work represents its first use in in a production wind tunnel tunnel. A discussion of background oriented schlieren and a brief review of relevant previous work follows. Processing techniques for BOS images are presented. We described data sets from two recent experiments and contrast their results. An historical data set, which was not optimized for the use of optical flow is also contrasted, demonstrating both the improvements achieved and the shortcomings associated with optical flow.

II. Background

Background oriented schlieren (BOS) imaging has seen increasingly wide spread use due to its versatility and relative ease of setup as opposed to classical schlieren systems. First detailed by Dalziel, Hughes,

*Research Engineer, ACI/Experimental Aero-Physics Branch, M/S 260-1, Member AIAA.
†Photographic Technologist, Experimental Aero-Physics Branch, M/S 260-1, Non-Member.
‡Aerospace Engineer, Experimental Aero-Physics Branch, M/S 260-1, Non-Member.

and Sutherland[3] an termed "synthetic schlieren", BOS relies on the visualization of a random background pattern shifted by the presence of a density gradient as compared to a quiescent background reference image. Richard and Raffel[4] expanded upon the technique, applying it to wind tunnel and full-scale flight experiments. Natural backgrounds were used by Kindler *et al.*[5] for rotor tip vortex measurements. Hargather and Settles later explored the natural background imaging technique extensively.[6] A thorough overview of BOS techniques and applications is provided by Raffel.[7]

Figure 1 shows the principle of BOS. When a light ray passes through a density gradient, the ray is deflected causing a distortion in the wind-on background pattern relative to the background pattern at wind-off conditions. The deflection of the light ray is directly proportional to the density gradient. BOS images are generated from the displacement data in the same way that particle image velocimetry image pairs are processed. The shift of the distorted background pattern relative to the reference image is typically detected using normalized cross-correlation and identifying peaks in the correlation map at the sub-pixel level. These detected shifts in the x and y directions are mapped to grayscale image values to create the schlieren image in the equivalent vertical knife edge dx and horizontal knife-edge dy.

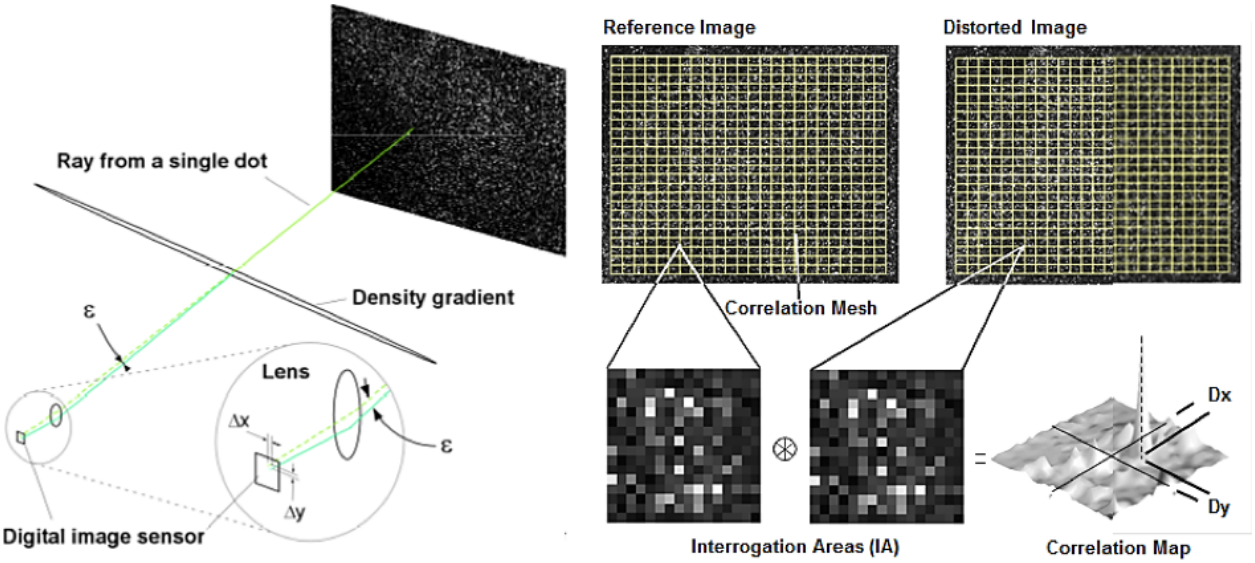

Figure 1. Illustration of the background oriented schlieren technique.

There exists a significant body of work regarding the application of optical flow and similar methods to particle image velocimetry *e.g.*,[8–11] meteorological flows,[12] and transmittency images of flows with contrast media.[13] Optical flow methods have also been used to study the motion between a schlieren image pair.[?,14] This is not the first use of optical flow to create BOS images. Hill and Haering[15] have had recent success in improving on the solar disk imagery as rendered by a Calcium-K line filter for ground-to-air visualization. This work pointed the authors to exploring optical flow more comprehensively. To the authors' knowledge, the only published study to use optical flow methods to generate BOS images was performed by Atcheson, Heidrich and Ihrke in 2009.[16] Yet nearly a decade on, the technique is not commonplace despite a compelling demonstration that it provides significantly more detailed qualitative images than normalized cross-correlation in simple experiments.

III. Processing Methods

The creation of a schlieren image from a background (wind-off) and flow (wind-on) image pair consists of three processing steps: registration of the flow image to the background (or vice versa), calculation of the displacement field between the registered image and the flow image, and finally a mapping of the displacements to image grayscale values. A second registration may be performed of the displacement images to a fixed wind-on reference in the sequence, creating a stacked time averaged image for multiple images of a steady state flow. Here, the displacement is calculated using both normalized cross-correlation and optical-flow methods.

Registration of the wind-on image to the background is accomplished by warping the flow image to the wind-off background using a transformation matrix. The projective (or perspective) transformation matrix is calculated from the sub-pixel resolved displacement of four manually selected regions as described in reference.[17] This transformation provides correction for any translation, rotation, zoom or tilting of the camera between image frames. A final registration may be performed to create a time averaged image of a sequence. This step may be performed in a number of ways including computing an additional warp, or an implementation of a computer vision-based tracking methodology.

A. Normalized Cross-Correlation

As in particle image velocimetry, normalized cross-correlation has become the method of choice for processing BOS data. Images are typically pre-processed with a high-pass filter prior to correlation. An interrogation grid is established, and the displacements between the wind-on and wind-off images are computed directly by image cross correlation at each node as illustrated in figure 1 on the previous page. The displacement is calculated using an interrogation window, the size of which is determined by a trade-off between the solution resolution and signal to noise ratio. Multi-grid strategies are typically employed, where coarse-to-fine interrogation windows are used successively to refine the solution. Sub-pixel displacement is typically calculated by fitting a Gaussian function through the local correlation peak. A more detailed discussion of these steps is presented in reference.[18] The resulting displacement components correspond to the dx and dy schlieren images, and are visualized by mapping pixel displacement to image grayscale levels.

B. Optical Flow

Optical flow, or the apparent motion between images due to brightness changes, is a well established technique developed by the computer vision community for motion estimation in image pairs and video. A topic of study in computer vision research for over three decades, numerous algorithms exist for the calculation of optical flow. The two most common motion estimation schemes are the local differential Lucas-Kanade[19] and the global differential Horn-Schunck[20] methods. This work uses the global regularization-based method of Horn and Schunck. This method was selected due its ability to solve the flowfield at every image point, a mathematical form that is intuitive to those with a fluid dynamics background, and the wide applicability of the method the authors have observed in their experience.

Irrespective of the implementation selected, optical flow has two major assumptions: the brightness of an object or pixel remains constant through the sequence, and the motion of an object between frames is small. This may be written below as

$$I\left(x,y,t\right) \approx I\left(x+\delta x, \delta y + y, t+\delta t\right) \tag{1}$$

where I is intensity image as a function of time and space, from which it follows that

$$\nabla I \cdot \mathbf{V} + I_t = 0 \tag{2}$$

where $\mathbf{V} = (u, v)$ is the image pixel velocity (or displacement) between frames, and the subscript t denotes differentiation with respect to time. Equation (2) is known as the brightness constraint equation; in effect, it represents the (assumed) conservation of brightness of a pixel undergoing a small motion between frames.

Equation (2) is under determined and requires a second constraint to solve. Horn and Schunck suggest an $L2$ norm of the velocity gradients as a smoothing function. The problem then becomes the minimization of a functional containing the brightness constraint in Equation (2) as the data term, and the $L2$-based velocity gradient regularizer (or smoothing term), over the image domain Ω given in Equation (3) below:

$$E = \int_{\Omega} \left\{ \left(\nabla I \cdot \mathbf{V} + I_t\right)^2 + \kappa^2 \left(\|\nabla u\|^2 + \|\nabla v\|^2 \right) \right\} d\Omega \tag{3}$$

In equation (3), the smoothness term is weighted by a constant κ; this is effectively a free parameter. The data term (from equation (2)) has a quadratic penalty function as originally proposed in.[20] Expanding equation (3), and applying the Euler-Lagrange equation yields the following system of equations:

$$\begin{aligned} I_x \left(I_x u + I_y v + I_t\right) &= \kappa^2 \nabla^2 u \\ I_y \left(I_x u + I_y v + I_t\right) &= \kappa^2 \nabla^2 v \end{aligned} \tag{4}$$

where subscripts denote partial differentiation in space and time. Recognizing that the Laplacian terms in the right hand sides of equations 4 on the preceding page (once discretized) involving u and v can be rewritten as $\bar{u}-u$ and $\bar{v}-v$ respectively, where $\bar{u}$ and $\bar{v}$ represent the off center terms of the five or nine-point Laplacian stencils, equation (4) can be written as

$$\begin{aligned} u &= \bar{u} - I_x \frac{I_x\bar{u} + I_y\bar{v} + I_t}{\kappa^2 + I_x^2 + I_y^2} \\ v &= \bar{v} - I_y \frac{I_x\bar{u} + I_y\bar{v} + I_t}{\kappa^2 + I_x^2 + I_y^2} \end{aligned} \tag{5}$$

The above system is a simple iterative scheme which may be solved by either a Jacobi or Gauss-Seidel iteration. We have implemented the former as it lends itself to straightforward parallelization.

C. Implementation

A Microsoft Windows application developed in house at the NASA Ames Fluid Mechanics Laboratory called *BOS_ETS* was used to calculate all normalized cross-correlation BOS images. This program also computes image registrations using a projective transform. To create a time-average image of a sequence (when possible), an additional correlation peak was tracked (for example on the moving target airplane for the flight-test data). Some of the results shown here using the normalized cross-correlation methods were originally presented in reference.[2]

All optical flow calculations were performed with a a separate code developed at the Fluid Mechanics Laboratory written in C++ and the OpenCV libraries. The existing Horn-Schunck algorithm written in OpenCV was not used, as it has limitations including numerical schemes (*e.g.* low order derivatives and data types) which make it poorly suited for an accurate and converged solution. Images were not smoothed prior to processing, as they were sharp and assumed to be noise free. Image spatial derivatives were calculated using 4th order accurate central differencing schemes as suggested by Barron, Fleet and Beauchemin.[21] A simple backward differencing yielded the temporal derivative. All image derivatives were calculated using an average of the derivatives of the wind-on and wind-off images. A nine-point two-dimensional stencil was used to calculate the Laplacian (without the center weighting term) as in reference.[20] Equations (5) were converged to to 10^{-6} using a non-normalized $L2$ criterion of the velocity components. Note that for most of the images, due to their large size, this resulted in a normalized converge near machine zero. It was found that a smoothness weighting κ of 10 provided the best tradeoff between solution sharpness and noise reduction in all test data sets. The program was parallelized on a desktop machine using the OpenMP v 3.0 application programming interface for shared memory architectures. The multi-core implementation allowed a reduction the optical-flow computational time by nearly and order of magnitude.

IV. Test Data

A. NASA AirBOS Flight Test Data

The flight-test data used in this paper is described in a recent publication by Heineck *et al.*,[2] which details a new method for BOS imaging of a full scale aircraft in flight termed "Air-to-Air BOS" (AirBOS). AirBOS images the target aircraft from an observation aircraft flying above it, and uses the natural flora on the ground as a speckle pattern to derive the schlieren imagery. The Mojave Desert flora of the Supersonic Corridor near Edwards Air Force Base provided a nearly ideal background. A schematic illustrating the AirBOS technique is shown in figure 2 on the next page. An observer instrumentation aircraft flies above the natural background. The target aircraft passes between the observer aircraft and the background; density gradients create a change in refractive index, distorting the background pattern relative to the wind-off image. As in standard BOS applications, this allows the calculation of the displacement between the image pairs (shown in figure 1 on page 2).

Two data sets from the flight campaign are used. In each case, the target T-38 aircraft is in supersonic flight at approximately Mach 1.05, and the observer aircraft is an altitude of approximately 30,000 ft. In the first sequence (referred to as pass 1), the vertical separation between the observer aircraft and the target aircraft is 5,000 ft. In pass 2 (the second sequence), the separation distance between the aircraft is reduced

to 2,000 ft., giving an effective magnification of the target aircraft. Two Phantom V641 cameras were used for data acquisition. Each sensor was 2560x1600 pixels with a 10 micron pitch. For contrast improvement and mitigation of atmospheric haze, A No. 25 Red glass filter was placed in front of each lens. Up to 45 reference frames were acquired prior to the target aircraft entering the observer aircraft field of view. The camera framing rate was varied between 500 and 1,400 frames per second, depending on separation distance between the observer and target aircraft, yielding between 150 and 500 wind-on images per flight pass. All images were taken with a $50\mu s$ exposure time. Representative raw images from the flight test of a wind-off and wind-on reference and a wind-on flow condition are shown in figure 3.

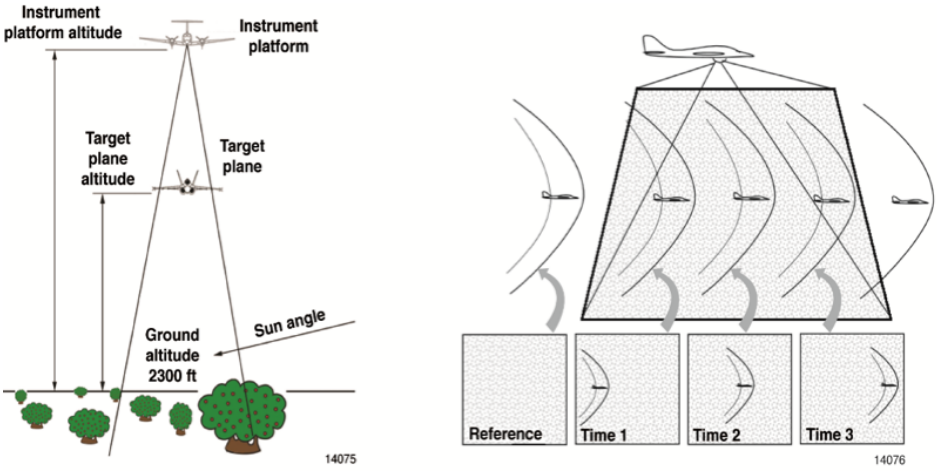

Figure 2. A schematic of the air-to-air background oriented schlieren technique.

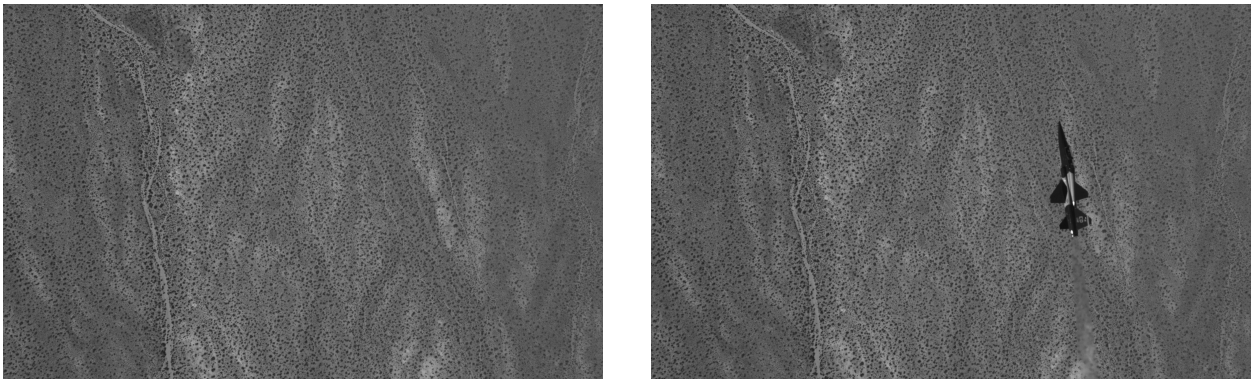

(a) Natural background wind-off reference image.

(b) T-38 aircraft wind-on flow image.

Figure 3. Raw images from the AirBOS flight test.

B. NASA Ames Plume/Shock Interaction Wind Tunnel Data

The wind tunnel data examined here is from the recent series of supersonic nozzle plume/shock interaction studies conducted in the 9-by 7-ft. Supersonic Wind Tunnel (SWT) at NASA Ames UPWT. The primary goal of the study was to examine the interactions of shocks impinging on a supersonic jet with an on-design exit Mach number of 2, to mimic those that may occur on the aft end of a low-boom supersonic aircraft. Multiple shock-generating geometries were studied at nominal freestream Mach numbers of 1.6 and 2 with varying nozzle pressure ratios. Durston *et al.*[1] provide a thorough description of the test. One of the optical access windows to the SWT test section was removed to place a pressure measurement rail in the tunnel, necessitating the use of a BOS imaging system. The retroreflective BOS image technique was used to obtain all schlieren images. The RBOS method[22] uses a random-speckled background that has been applied to an adhesive retroreflective material. The advantages of the RBOS method are twofold: first, the retroreflective

material creates more efficient use of illumination, and second, in part due to the reflective material, the method is easier to set up when optical access and spatial constraints are an issue in the test section. The supersonic nozzle model as installed in the SWT test section is shown in figure 4, note the high pressure nozzle body mounted on the model sting. The retroreflective background material can be seen on the lower half of the schlieren window blank beneath the pressure rail in figure 4 below.

The cameras used for the recording of the reference and data images were Imperx B6620 29 Mpix cameras. The pixel pitch is 4.7 microns and the array dimension is 6576x4384. Cameras were fitted with a Zeiss ZF 85 mm lens set to f22 and operated at approximately 2 Hz. To satisfy the brightness constancy assumption in equation (2) and provide validity to the optical-flow method, a constant illumination source was required. In addition, optical flow performs poorly when objects are occluded. This required the mitigation of any hard shadows. To provide the necessary even illumination and soften shadows, a diffuse ring illumination source was installed.

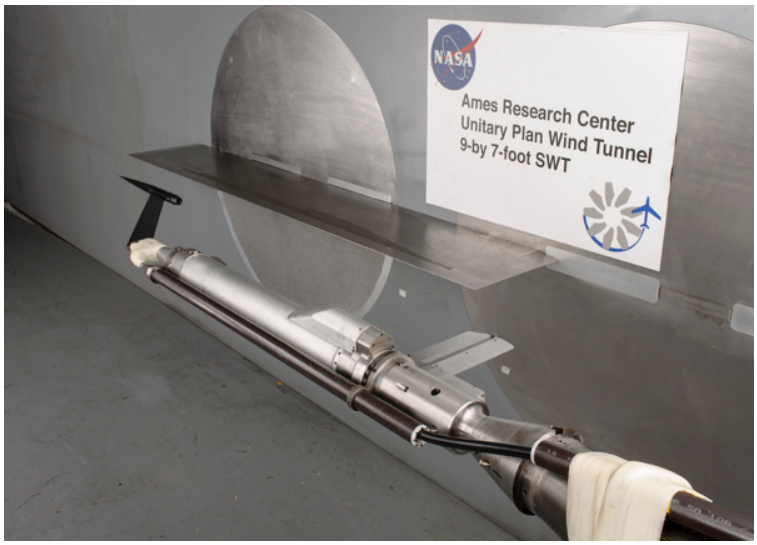

Figure 4. The nozzle plume/shock interaction model as installed in the NASA Ames 9x7 SWT.

The data presented here focuses on two geometries shown in figure 5. The aft-deck (figure 5(a)), which was mounted beneath the nozzle exit plane, and the double-wedge (diamond) airfoil (figure 5(b)) mounted above the nozzle exit plane in such a manner that the resulting shock and expansion waves impinge on the nozzle plume. A representative wind-off wind-on image pair of the raw data are shown in figure 6 on the next page for the double-wedge shock-generator. Note that the shadows cast by the model are present in the reference image to prevent violations of brightness constancy in the optical flow equation.

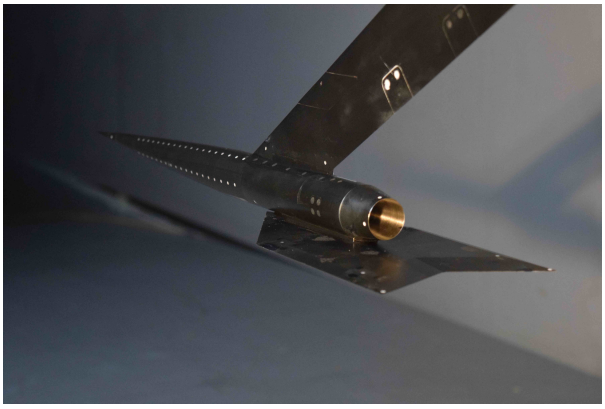

(a) Aft-deck nozzle shielding model.

(b) Double-wedge tail shock-generator model.

Figure 5. Example shock-generating geometries from the NASA plume/shock interaction tests.

(a) Double-wedge airfoil wind-off reference image.

(b) Double-wedge airfoil wind-on flow image.

Figure 6. Raw images from the RBOS wind-tunnel test. Note the model shadows are captured in both the flow and reference images.

V. Results and Discussion

A. Flight Test Results

During the analysis of the data, it was noticed that the use of multiple distinct background images has the potential to reduce noise in the optical flow solution and remove Moiré patterns that may result from registration and aliasing errors. Approximately 45 images were available for use as references from each flight pass. To determine a trade off between solution time and noise reduction, a single image from each pass was registered to all 45 reference images. The optical flow was calculated for each registration, accumulated and normalized. A standard deviation was calculated in a 256x256 region of interest (ROI) of the accumulated optical flow in the freestream ahead of the airplane, as this should ideally converge to a constant value. The results of this study are shown in Figure figure 7, where standard deviation of the freestream ROI is plotted against the number of reference images used. Note that for both cases, the standard deviation drops most rapidly within the first 5 images (approximately 20%). Although the standard deviation continues to drop and does not approach an asymptote until 25 images are used, the additional decrease in standard deviation offers a relatively meager 5% improvement. As computation time increases linearly with the number of optical flow calculations, figure 7 indicates that the best compromise is reached when five references are used. All the following AirBOS images calculated using optical flow have been registered against five background images. Comparison between solutions calculated with one and five references showed that a significant Moiré pattern was removed, and that the freestream region noise had decreased. This is consistent with the findings presented in figure 7.

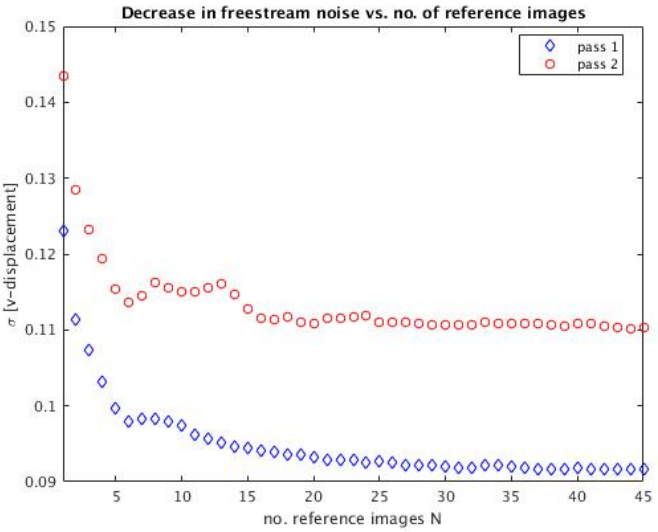

Figure 7. Effect of using multiple reference images.

1. *Flight pass 1: 5,000 ft. aircraft separation distance.*

Figure 8 on page 9 shows the schlieren images from a single time instance compared against a single reference for the pass 1 flight where the aircraft are separated by 5,000 ft. The topmost schlieren image was obtained using normalized cross correlation, and the bottom was computed using optical flow. While neither image is particularly clear, the cross-correlation image in figure 8(a) on page 9 appears blurred as compared to its

optical-flow counterpart in figure 8(a) on the next page. Shocks are more distinct and the region surrounding the aircraft is more detailed in the optical-flow image. The aircraft itself appears as pure noise, this is because the aircraft is not present in the reference image. The noise bands near the image edges are due to the motion of the aircraft from the reference wind-off image to the flow wind-on image. It should be noted that the plume is not a displacement solution; the exhaust distorts and occludes the corresponding region in the reference images, rendering this area unsolvable by either method. These observations regarding image noise obscuring the plume region apply to all subsequent images in this section.

The full time-averaged sequence from pass 1 is shown in figure 9 on page 10. Each is a composite of approximately 200 images; the cross-correlation solution in figure 9(a) on page 10 has been referenced against a single image, and each image was registered to five references for the optical flow solution in figure 9(b) on page 10. Alignment was accomplished for the cross-correlation solution by tracking a sun glint on the target aircraft using normalized cross-correlation. This allowed each image to be aligned to a centered image using a linear correction. To create a time-average image from the optical flow results, a separate sparse tracking optical flow method (Lucas-Kanade[19]) as implemented in OpenCV, was used to track several points on the target aircraft. Note that this final tracking method for alignment of the T-38 images may be accomplished by any number of means. The time-averaged schlieren images in figures 9(a) on page 10 and 9(b) on page 10 are significantly clearer than their single-image counterparts, due in large part to the increased signal-to-noise ratio provided by the averaging. Inspection of the optical-flow solution shows that greater detail of the flowfield is achieved over cross correlation, in particular, the wave structures around the aircraft are clearer, and the recompression near the canopy in figure 9(b) on page 10 is absent from the cross-correlation solution in figure 9(a) on page 10. Note also that the wave structures at the image borders remain distinct further away from the aircraft in the optical flow solution.

2. Flight pass 2: 2,000 ft. aircraft separation distance.

Figures 10 on page 11 and 11 on page 12 show the AirBOS flight pass with a reduced separation distance between the target and observer aircraft. The reduction of the distance between the T-38 aircraft and the chase airplane reveals much greater flow details of the near field, but sacrifices wave structures in the mid field. In the single image solutions, both methods show Mach wave radiation emitting from the plume boundaries, although this is easier to see in the optical-flow results. Note the large wave structures near the canopy and tail in figure 10(a) on page 11 are revealed to be multiple distinct waves by the optical flow solution in figure 10(b) on page 11. Nearly 400 images were used to create the time-averaged images in figure 11 on page 12, noise cancellation has revealed extremely detailed flowfields for both the cross-correlation and optical-flow results. The T-38 aircraft has been overlaid on the cross-correlation solution in figure 11(a) on page 12, but not in figure 11(b) on page 12, although the noise reduction has revealed distinct features on the aircraft. The shock forming at the pitot probe on the aircraft nose section was not captured using cross correlation, but is shown in the optical-flow result. The optical-flow image illustrates fine details of the flowfield; the flow recompression downstream of the nose is visualized, and the flow over the canopy reveals the expected wave details of compressible flow over a curved surface. The Mach wave radiation from the plume evident in the single images has been removed in the time-averaged images as expected. The improvement in the optical flow solution resolution exhibited so far can be attributed to the fact that optical flow solves for displacement at every image point. Cross-correlation calculations rely on window displacements. This template matching of windows effectively down-samples the image by a factor of the finest correlation window size used.

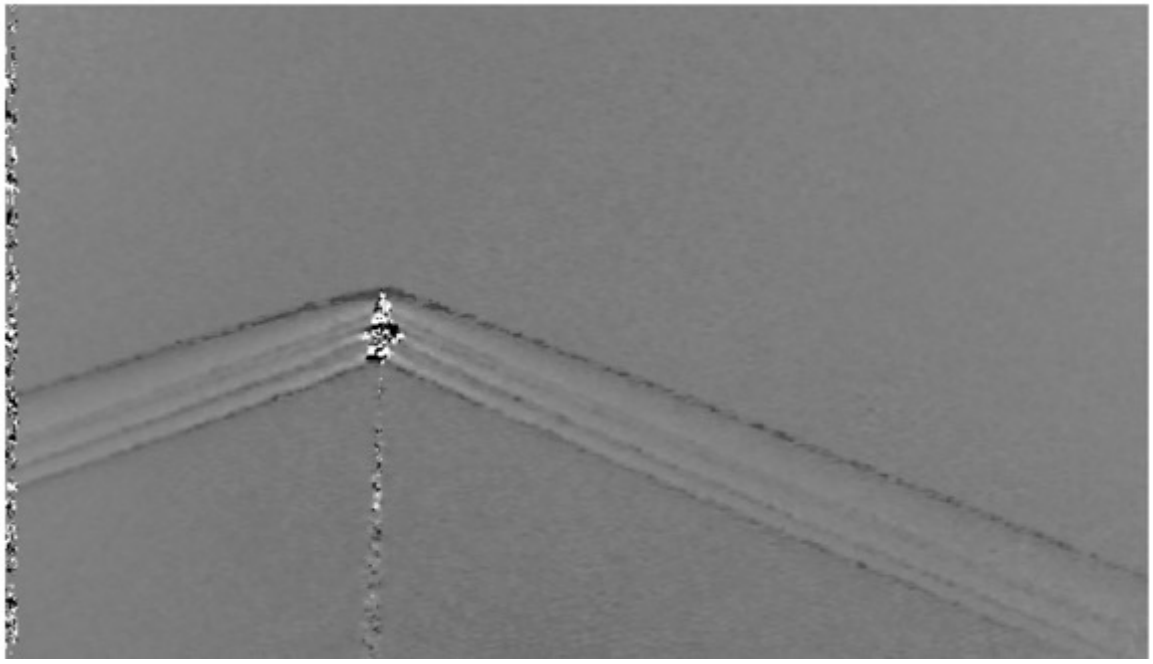

(a) Normalized cross-correlation result.

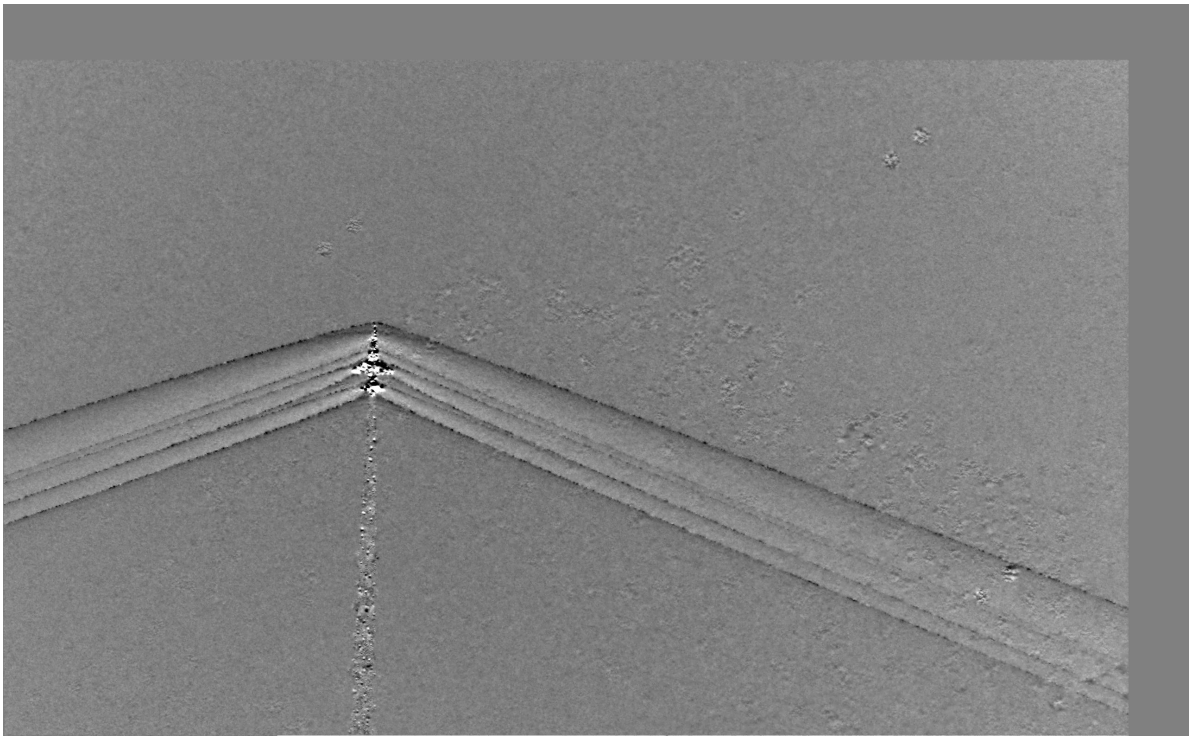

(b) Optical flow result.

Figure 8. AirBOS pass 1 schlieren images for a single image pair, *dy* knife-edge shown. Target and observer aircraft separated by 5,000 ft.

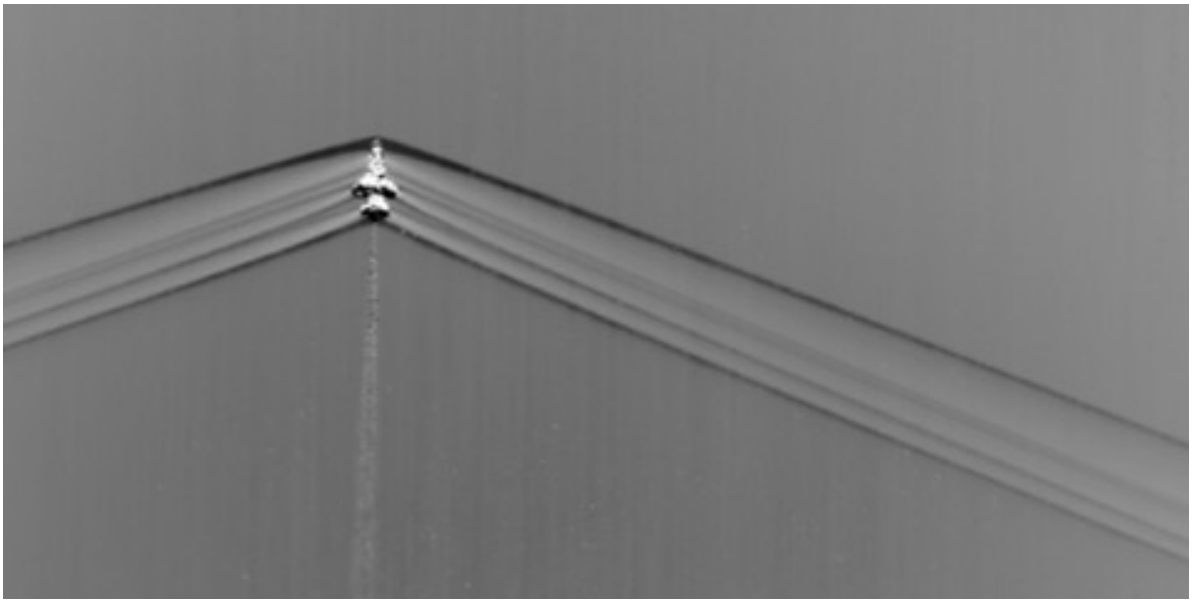

(a) Normalized cross-correlation result.

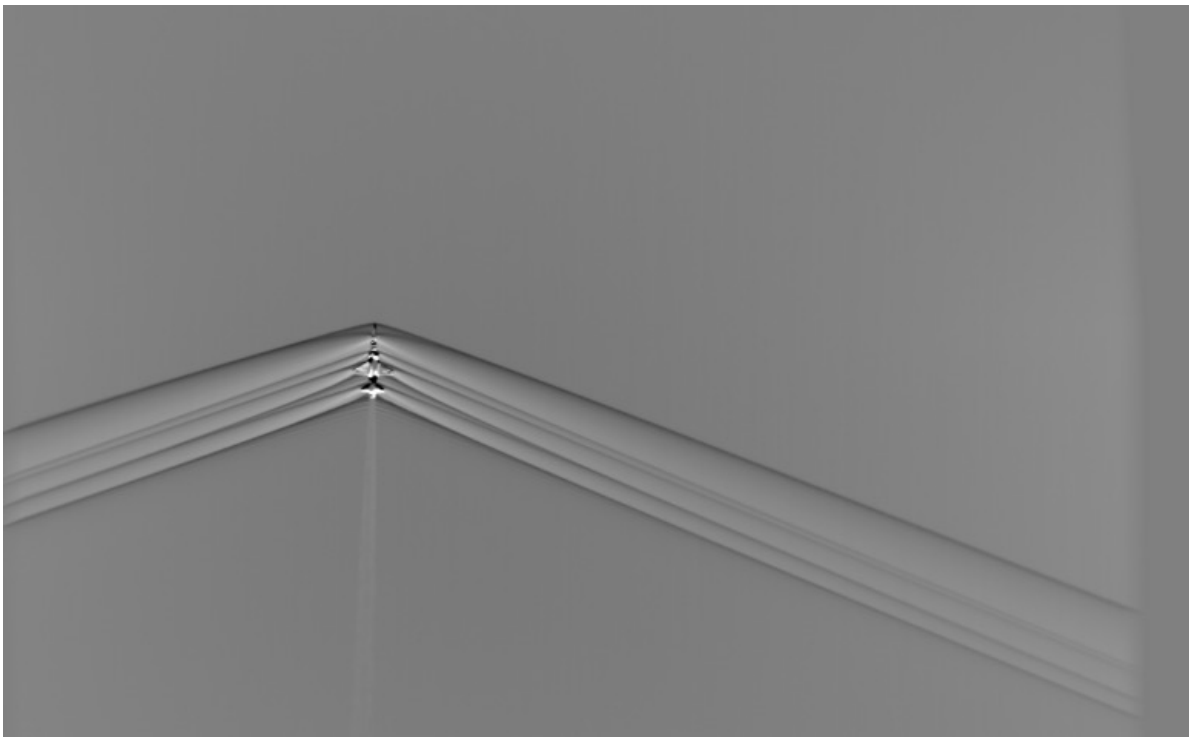

(b) Optical flow result.

Figure 9. AirBOS pass 1 schlieren time-averaged full sequence images, dy knife-edge shown. Target and observer aircraft separated by 5,000 ft.

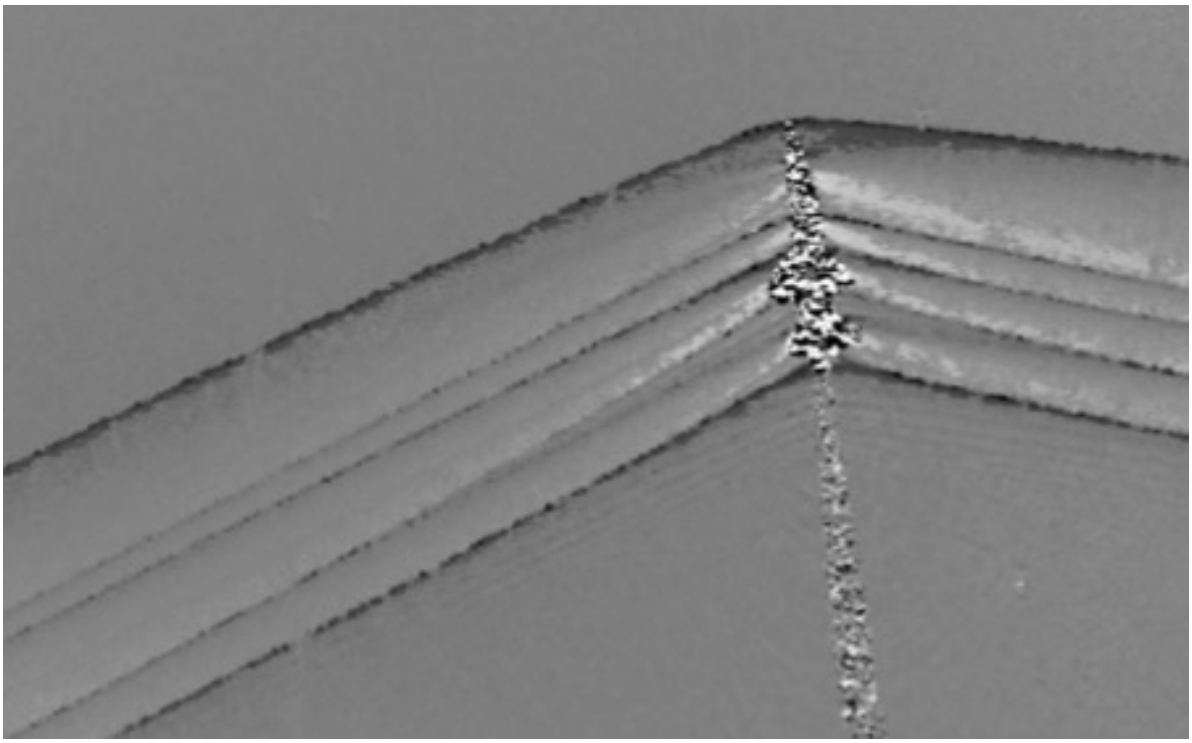

(a) Normalized cross-correlation result.

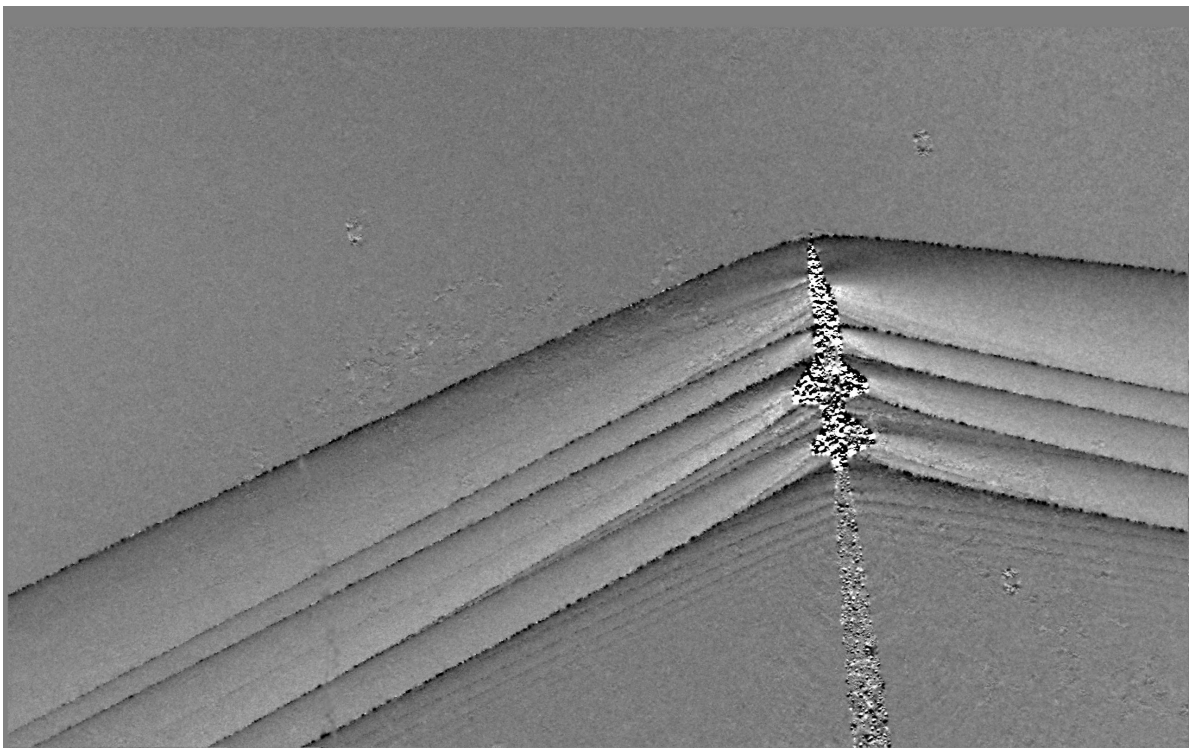

(b) Optical-flow result.

Figure 10. AirBOS pass 2 schlieren images for a single image pair, dy knife-edge shown. Target and observer aircraft separated by 2,000 ft.

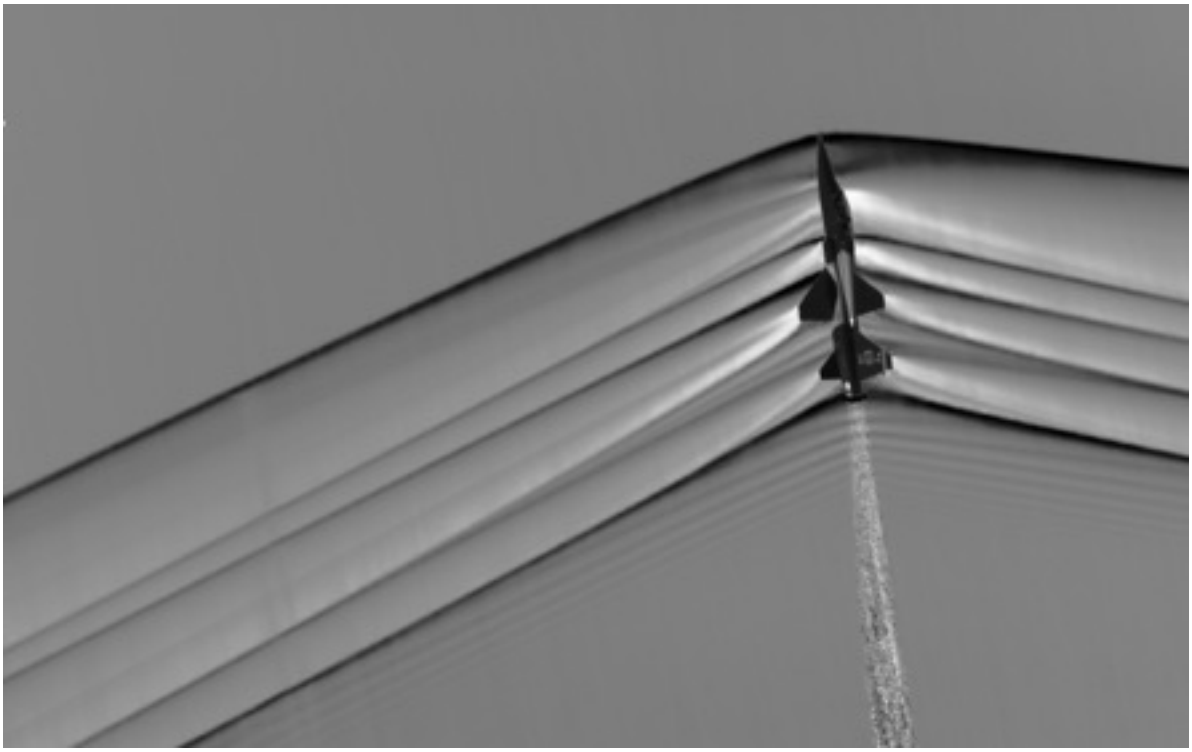

(a) Normalized cross-correlation result.

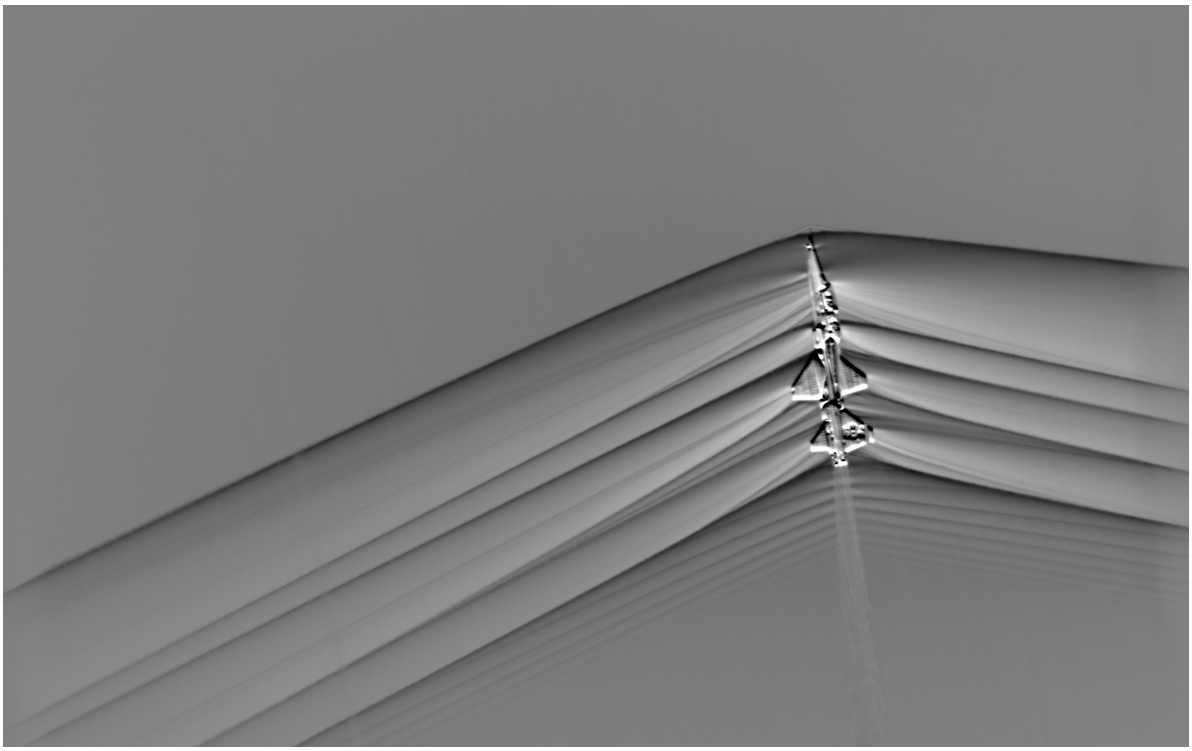

(b) Optical flow result.

Figure 11. AirBOS pass 2 schlieren time-averaged full sequence images, *dy* knife-edge shown. Target and observer aircraft separated by 2,000 ft.

B. Wind Tunnel Results

Multiple background images were acquired for each shock-generating configuration during the nozzle plume/shock interaction tests. It was assumed beforehand that tunnel vibration would cause enough camera motion such that individual background images would be distinct (*e.g.* significantly different renderings, as seen during the AirBOS flight passes). During the data reduction process, it was noticed that the background images were not sufficiently different to create the desired aliasing effect that leads to the desired noise cancellation. Therefore, the optical flow solution for each RBOS image was calculated against a single reference. Significant motion of the test assembly (shown in figure 4 on page 6) was observed during testing. Due to the model motion, and the model lacking any trackable points that could be viewed by the diffuse lighting of the schlieren system (the configurations were painted matte black for a simultaneous optical measurement), the time averaged images could not be accurately aligned using an additional registration step. All images presented in this section are simply an average of 10 time instances.

1. Aft-deck plume/shock interaction

Schlieren image results are shown for the aft-deck nozzle plume/shock interaction configuration in figure 12 on the next page. The aft-deck configuration was designed to divert the downward directed nozzle lip shock upward. This test case was run at a freestream Mach number of 2 with a Reynolds number of $3.5\text{x}10^6$/ft, and the nozzle is operating in the under-expanded regime. There is considerably more detail in the optical-flow rendering (figure 12(b) on the following page) of the freestream data than the cross-correlation counterpart (figure 12(b) on the next page). Additional wave structures are revealed by optical flow; namely the unsteady compression waves that are characteristic of the freestream in the SWT. The optical flow solution of aft-deck interaction in figure 12 on the following page has clarified additional flow details in the plume structure, particularly in the under-expansion nozzle region. The downward directed centerline and trailing edge shocks are more distinct, and an upward directed trailing edge shock has been revealed that was difficult to view in the cross-correlation solution.

2. Double-wedge airfoil plume/shock interaction

Figure 13 shows the plume/diamond airfoil shock interaction at a freestream Mach number of 2. The nozzle is operating in the under-expanded region and the intersecting expansion fans are well defined, as well as the nozzle outer lip shocks. The shock and expansion structures are clearly captured on the diamond airfoil shock generator above the plume. The differences in the solutions of the plume/shock interaction in figure 13 on page 15 are particularly pronounced in this region. The boundaries of the centered expansion fan from the diamond airfoil are much clearer in the optical flow solution, as is the expansion fan reflecting from the plume upper boundary and its effect of turning the plume. Both the leading and trailing edge shocks are deflected as they pass through the plume. Both the plume boundaries and the wake from the double-wedge airfoil are more defined in the optical flow solution in figure 13(b) on page 15. Note that portions of the leading and trailing edge shocks from the double-wedge geometry do not seem to change as they pass through the plume. These are portions of the shocks that pass on either side of the plume due to the large span of the model, and are a three-dimensional effect. The improved clarity in the optical flow solution is again attributed to lack of effective image down-sampling caused by template windows required for cross correlation. The Improved solution resolution is not without its caveats; note the small noise bands above and below the nozzle. These are caused by the shadows cast by the nozzle body in figure 6(b) on page 7. Although care was taken to reduce hard shadows, their effects have not been removed entirely.

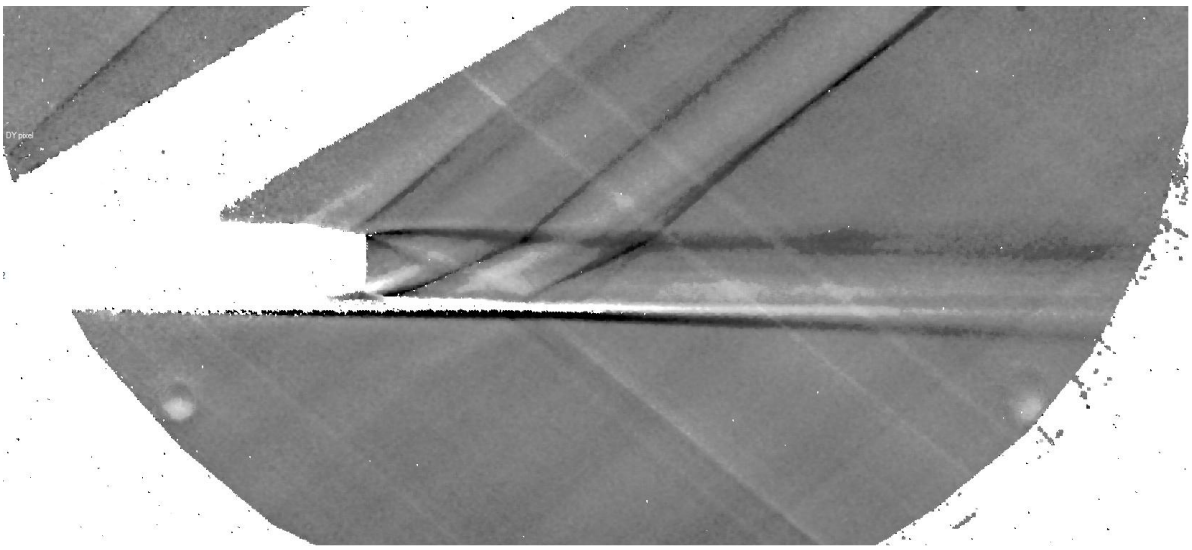

(a) Normalized cross-correlation result.

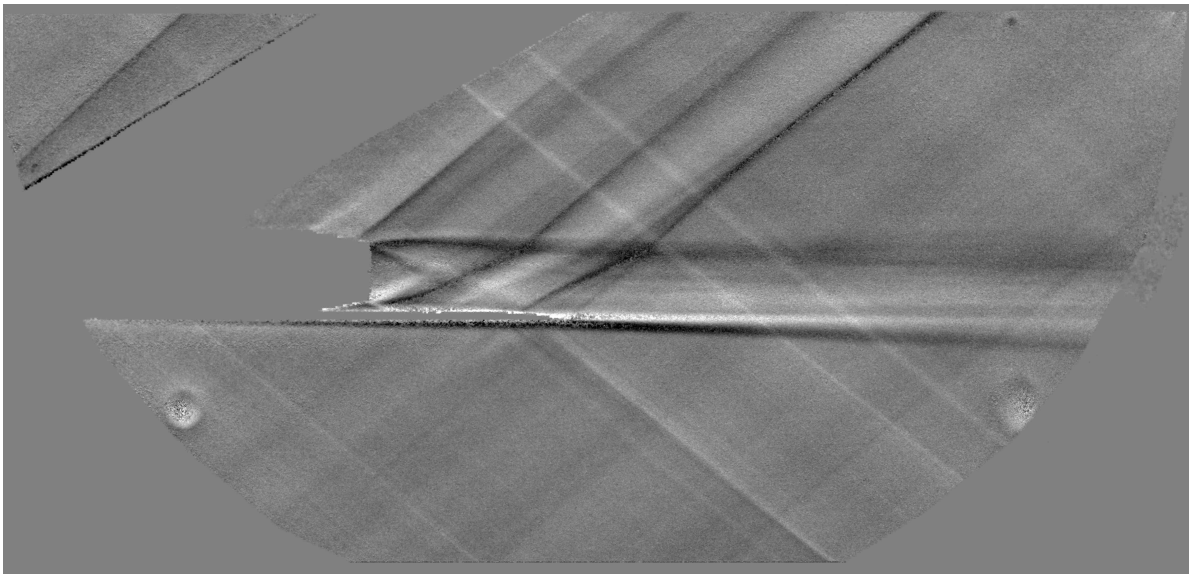

(b) Optical flow result.

Figure 12. Nozzle plume/aft-deck shock interaction. Each image is an average of 10 time instances.

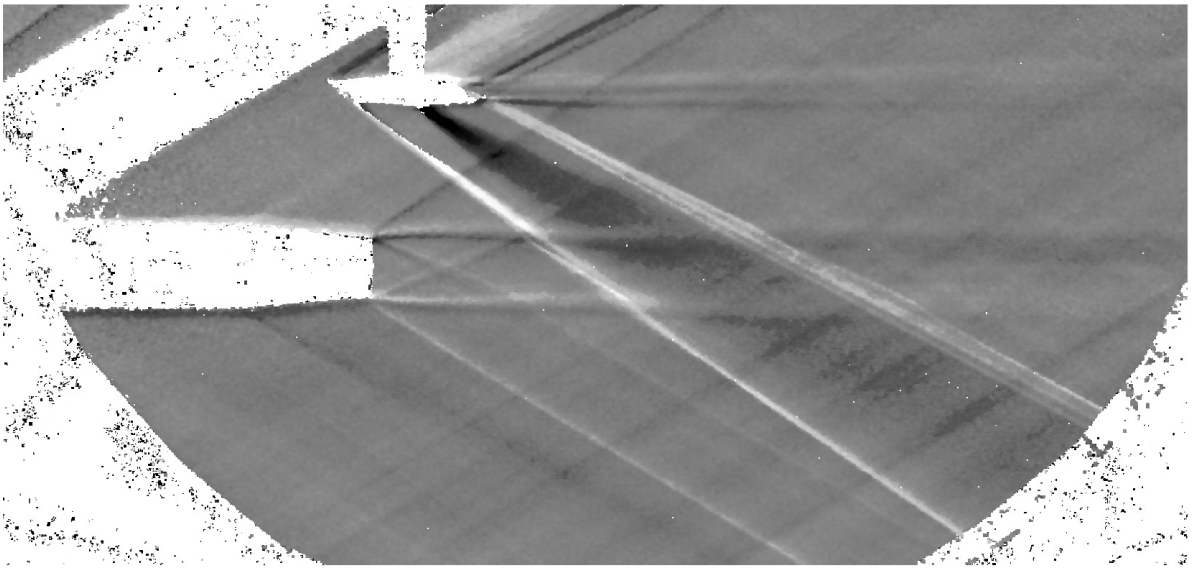

(a) Normalized cross-correlation result.

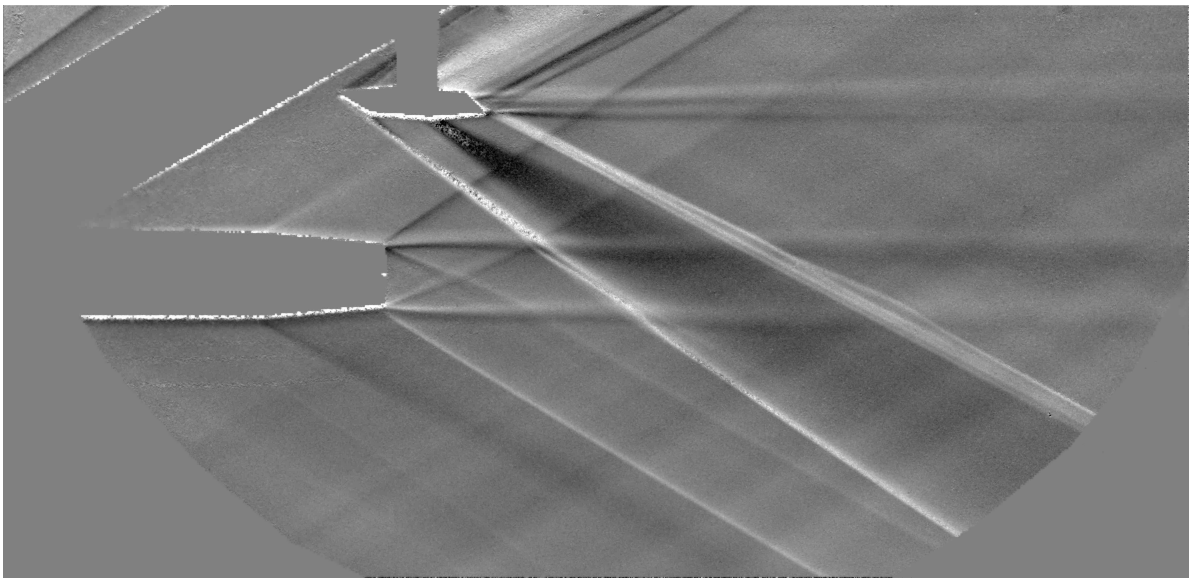

(b) Optical flow result.

Figure 13. Nozzle plume/diamond airfoil shock interaction. Each image is an average of 10 time instances.

3. Delta wing wind-tunnel results.

Figure 14 shows the wind-off reference and wind-on flow raw images from a test of a small delta wing model in the NASA Ames 9x7 SWT. These RBOS results were part of a test to study measurement techniques for sonic boom measurements in 2012 which were not previously published. It was not planned at the time to use optical flow during for data reduction, so the wind-off reference image was therefore taken without the model in place. Note also in figure 14(b) that a diffuse ring illumination source was not used, and hard shadows were cast by the model and sting assembly. Results from cross-correlation and optical flow are shown in figure 15. The model and sting areas were masked for the cross-correlation calculation, but not for the optical flow. The gross-flow features are captured well in the solutions for each method. Two features stand out for comparison in the figure. Firstly, the optical flow has once more provided much greater detail, particularly in capturing the unsteady compression waves in the free stream. This is again due to the fact that optical flow provided a solution at every image pixel (where the brightness constancy constraint is valid). Secondly, optical flow has completely failed to solve any portion of the shadowed region. While cross-correlation has not entirely solved the shadowed region, the trailing edge wakes on the body have not been obscured.

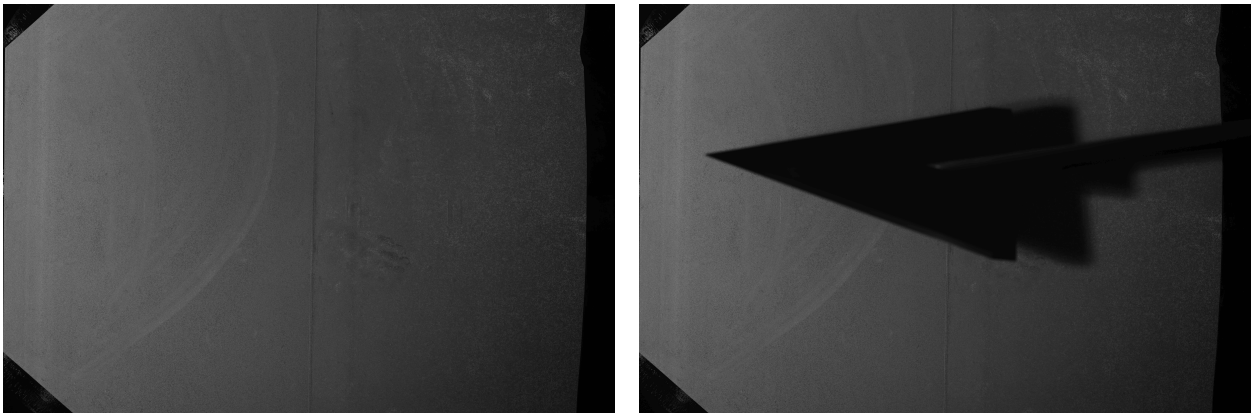

(a) Wind-off delta wing background image.

(b) Wind-on delta wing flow image.

Figure 14. Delta wing test raw data.

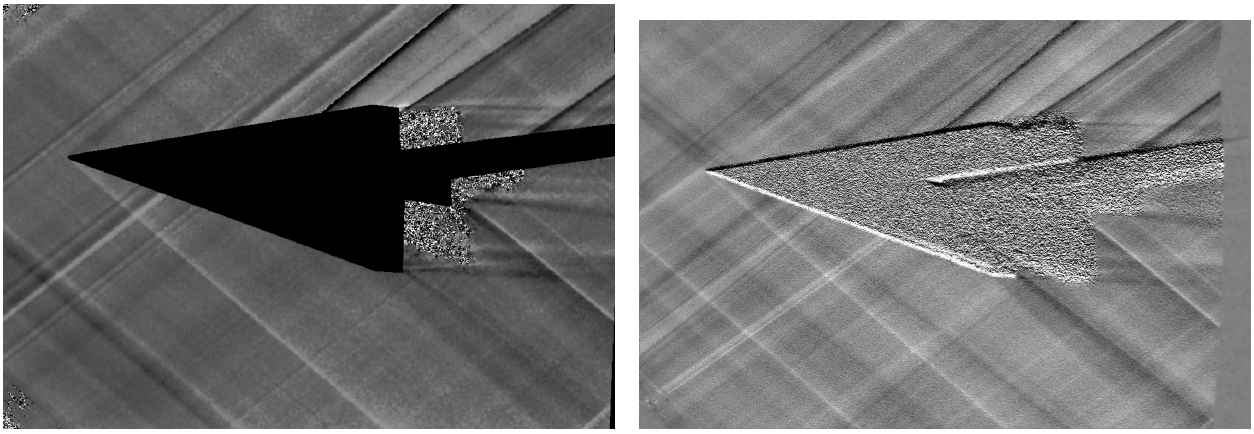

(a) Normalized cross-correlation result.

(b) Optical flow result.

Figure 15. Delta wing result. Each image is a single time instance.

VI. Conclusions

Optical flow techniques have been used to process both wind tunnel retroreflective BOS and in-flight natural background BOS data. The optical-flow methods have provided the highest quality AirBOS results obtained to date. As compared to standard cross-correlation methods, both the instantaneous and the sequence averages given by the optical-flow results yielded much finer flow structures in the flight data, particularly in revealing the complex expansion and compression waves near the aircraft canopy, and the delineation of the vertical and horizontal tail waves. A study of multiple distinct background images reveals that the use of multiple references can decrease noise in the computed flow images, and that the improvement with multiple reference images approaches an asymptote after five images. As expected, and as with previous cross-correlation studies, we found that flow structure detail improves significantly with decreased separation between the observer and target aircraft. This work is the first instance of optical flow used to provided BOS images in a production wind-tunnel test at NASA Ames Research Center. Optical-flow images provided details of the plume/shock interaction valuable to the computational fluid dynamics community that the normalized cross-correlation images could not. Such flow features included the details of the of the unsteady freestream compression waves and finer resolution of the interaction of wave structures with the plume. The increased flowfield clarity that results from optical flow is largely due the fact that window matching is not required as in normalized cross-correlation. This results in a displacement solution at every pixel as opposed to the effective down-sampling that results from the correlation mesh.

For wind-tunnel applications, it was noticed that optical flow algorithms are less robust than cross-correlation in the presence of shadows; the algorithm has difficulty resolving occlusions. This was expected prior to the RBOS installation, and was mitigated to an extent by the use of a diffuse ring illumination system. Optical flow was also demonstrated on a data set where lighting considerations were not taken into account, and showed an increase in solution accuracy, but a failure to capture important flow structures in the region of hard shadows. Optical flow is also much lest robust to changes in brightness between wind-off reference and wind-on flow images than cross correlation. Light sources for BOS setups when optical flow is intended to be used should attempt to address these issues by eliminating as much shadow as possible during wind tunnel installation, and make use of consistent illumination sources.

Acknowledgements

The authors would like to acknowledge Bron Nelson from the Systems and Engineering Branch and Chris Henze from the Computational Technologies Branch at the NASA Advanced Supercomputing (NAS) Division for their considerable guidance during the code development phase of this research.

References

[1]Durston, D. A., Cliff, S. E., Denison, M. F., Smith, N. T., Heineck, J. T., Schairer, E. T., Kushner, L. K., Castner, R. S., Elmiligui, A. A., Carter, M. B., Winski, C. S., Shea, P. R., and Blumenthal, B. T., chap. Nozzle Plume/Shock Interaction Sonic Boom Test Results from the NASA Ames 9- by 7-Foot Supersonic Wind Tunnel, AIAA Science and Technology, American Institute of Aeronautics and Astronautics, Janurary 2017.

[2]Heineck, J. T., Banks, D., Schairer, E. T., Haering, E. A., and Bean, P., chap. Background Oriented Schlieren (BOS) of a Supersonic Aircraft in Flight, AIAA Aviation, American Institute of Aeronautics and Astronautics, Jun 2016.

[3]Dalziel, S. B., Hughes, G. O., and Sutherland, B. R., "Synthetic schlieren," *Proc. 8th Int. Symp. on Flow Visualization*, 1998.

[4]Richard, H. and Raffel, M., "Principle and applications of the background oriented schlieren (BOS) method," *Measurement Science and Technology*, Vol. 12, No. 9, 2001, pp. 1576.

[5]Kindler, K., Goldhahn, E., Leopold, F., and Raffel, M., "Recent developments in background oriented Schlieren methods for rotor blade tip vortex measurements," *Experiments in Fluids*, Vol. 43, No. 2, 2007, pp. 233–240.

[6]Hargather, M. J. and Settles, G. S., "Natural-background-oriented schlieren imaging," *Experiments in Fluids*, Vol. 48, No. 1, 2010, pp. 59–68.

[7]Raffel, M., "Background-oriented schlieren (BOS) techniques," *Experiments in Fluids*, Vol. 56, No. 3, 2015, pp. 60.

[8]Ruhnau, P., Kohlberger, T., Schnörr, C., and Nobach, H., "Variational optical flow estimation for particle image velocimetry," *Experiments in Fluids*, Vol. 38, No. 1, 2005, pp. 21–32.

[9]LIU, T. and SHEN, L., "Fluid flow and optical flow," *Journal of Fluid Mechanics*, Vol. 614, 11 2008, pp. 253–291.

[10]Liu, T., Merat, A., Makhmalbaf, M. H. M., Fajardo, C., and Merati, P., "Comparison between optical flow and cross-correlation methods for extraction of velocity fields from particle images," *Experiments in Fluids*, Vol. 56, No. 8, 2015, pp. 166.

[11]Corpetti, T., Heitz, D., Arroyo, G., Mémin, E., and Santa-Cruz, A., "Fluid experimental flow estimation based on an optical-flow scheme," *Experiments in Fluids*, Vol. 40, No. 1, 2006, pp. 80–97.

[12]Corpetti, T., Memin, E., and Perez, P., "Dense estimation of fluid flows," *IEEE Transactions on Pattern Analysis and Machine Intelligence*, Vol. 24, No. 3, Mar 2002, pp. 365–380.

[13]Wildes, R. P., Lanzillotto, A. M., Amabile, M. J., and Leu, T.-S., "Physically based fluid flow recovery from image sequences," *Computer Vision and Pattern Recognition, 1997. Proceedings., 1997 IEEE Computer Society Conference on*, Jun 1997, pp. 969–975.

[14]Arnaud, E., Mémin, E., Sosa, R., and Artana, G., "A Fluid Motion Estimator for Schlieren Image Velocimetry," *Proceedings of the 9th European Conference on Computer Vision - Volume Part I*, ECCV'06, Springer-Verlag, Berlin, Heidelberg, 2006, pp. 198–210.

[15]Hill, M. A. and Jr., E. H., "Ground to Air Flow Visualization Using Solar Calcium-K line Background Oriented Schlieren," *accepted for publication in Experiments in Fluids*, 2017.

[16]Atcheson, B., Heidrich, W., and Ihrke, I., "An evaluation of optical flow algorithms for background oriented schlieren imaging," *Experiments in Fluids*, Vol. 46, No. 3, 2009, pp. 467–476.

[17]Bell, J. H. and McLachlan, B. G., "Image registration for pressure-sensitive paint applications," *Experiments in Fluids*, Vol. 22, No. 1, 1996, pp. 78–86.

[18]Raffel, M., Willert, C. E., Wereley, S., and Kompenhans, J., *Particle image velocimetry: a practical guide*, Springer, 2013.

[19]Lucas, B. D., Kanade, T., et al., "An iterative image registration technique with an application to stereo vision." *IJCAI*, Vol. 81, 1981, pp. 674–679.

[20]Horn, B. K. and Schunck, B. G., "Determining optical flow," *Artificial intelligence*, Vol. 17, No. 1-3, 1981, pp. 185–203.

[21]Barron, J. L., Fleet, D. J., and Beauchemin, S. S., "Performance of optical flow techniques," *International Journal of Computer Vision*, Vol. 12, No. 1, 1994, pp. 43–77.

[22]Heineck, J. T., Schairer, E. T., Walker, L., and Kushner, L., "Retroreflective background oriented schlieren (rbos)," *Proceedings of the 14th international symposium on flow visualization (ISFV14), EXCO Daegu, Korea*, 2010.